An Investigation of the Chromium Oxidation State of a Monoanionic Chromium Tris(catecholate) Complex by X-ray Absorption and EPR Spectroscopies

David I. Pattison,[†] Aviva Levina,[†] Michael J. Davies,[‡] and Peter A. Lay*[,†]

Centre for Heavy Metals Research, School of Chemistry, University of Sydney, Sydney, NSW 2006, Australia, and The Heart Research Institute, 145 Missenden Road, Camperdown, Sydney, NSW 2050, Australia

Received March 20, 2000

The well-known monoanionic Cr tris(3,5-di-*tert*-butylcatecholato) complex, $[Cr(DTBC)_3]^-$, has been studied by X-ray absorption spectroscopy. The multiple-scattering fit to the XAFS gave good correlation ($R = 19.8\%$) and good values for all of the bond lengths, angles, and Debye−Waller factors. The principal bond lengths and angles around the metal center (Cr−O, 1.96 Å; O−C, 1.28 Å; O−Cr−O, 81.8°; Cr−O−C, 113.3°) were most consistent with the XRD structure for $[Cr(X_4C_6O_2)_3]^-$ (X = Cl, Br), compared to those in other oxidation states, $[Cr(DTBC)_3]$, $[Cr(Cl_4C_6O_2)_3]$, and $[Cr(O_2C_6H_4)_3]^{3-}$. The XANES spectrum shows the main K edge at 6003.3 eV and a preedge peak at 5992.9 eV, which is ∼8% of the intensity of the main K edge. The XANES data were compared to those for Cr−ehba complexes (ehbaH_2 = 2-ethyl-2-hydroxybutanoic acid) of known oxidation states (III, IV, and V) and show, in conjunction with EPR spectroscopy and a reevaluation of XRD structures and theoretical calulations, that the complex is best described as a Cr(V) center with delocalization from the catechol ligands. The $[Cr(catecholato)_3]^{n+}$ ($n = 1, 0$) complexes have similar EPR spectroscopic and structural properties, respectively, to the 1− complex and are also best described as Cr(V) complexes. Such intermediates are important in the redox reactions of catechol(amine)s, and oxidized amino acids (e.g., DOPA), with carcinogenic Cr(VI) and may have relevance in Cr-induced cancers.

Introduction

Complexes with redox-active catechol ligands (eqs 1 and 2), $[M(cat)_3]^n$ (M = Cr, Fe, V), have been used as model compounds for the microbial iron transport reagents, enterobactin.[1−4] In the seven-membered Cr redox series, the overall charge varies from 3+ to 3− (Scheme 1).[5,6] Theoretical studies have predicted that the monoanionic and monocationic species both have single unpaired electrons,[7] which has been confirmed by magnetic measurements and EPR spectroscopy.[5,6]

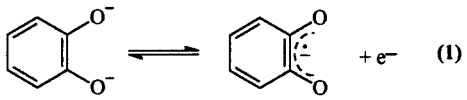

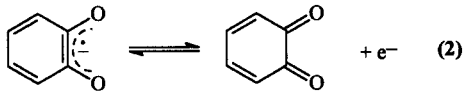

Calculations indicate that the molecular orbitals are delocalized over the metal center and at least one of the ligands.[7] The variation in charge is postulated to originate from oxidation/reduction of the ligands (catecholate, semiquinone, or quinone) with the oxidation state remaining as Cr(III) throughout the redox series,[5,6,8] as deduced from X-ray crystallography.[2,5,6,8,9] Such a model conflicts with the narrow EPR signals at $g_{iso} \sim 1.972$ (line width (LW) = $2-10 \times 10^{-4}$ cm^{-1}) observed for both the monoanionic and monocationic species,[5,6] which are typical of Cr(V) species.[10,11] By contrast, octahedral Cr(III) complexes typically give broad signals (LW > 1×10^{-2} cm^{-1}) at $g_{iso} \sim 1.98$.[12,13] From previous EPR studies of [Cr(3,6-di-*tert*-butylcatechol)$_3$]^n ($n = 1+, 1-$), it was deduced that the charge on Cr was invariant (+3.7 electrons) among monocation, monoanion, and uncharged species.[14]

The position and shape of the preedge region of Cr X-ray absorption spectra depend on the Cr oxidation state;[15,16] hence XAS studies on K[Cr(DTBC)$_3$] (DTBC = 3,5-di-*tert*-butylcatechol) were investigated. The resultant information on the

Scheme 1. Summary of the Redox Chemistry of Cr Tris(catecholate) Complexes[a]

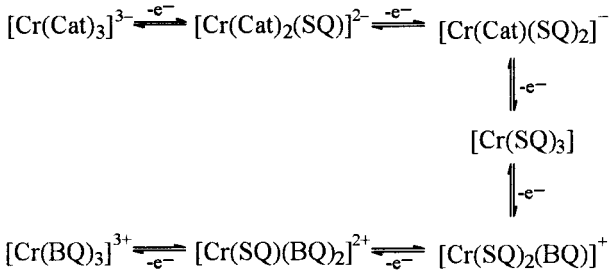

[a] The ligand states (Cat = catecholate; SQ = semiquinone; BQ = quinone) are assigned assuming that the metal center remains in the Cr(III) oxidation state throughout the series.[5]

[†] University of Sydney.
[‡] The Heart Research Institute.

(1) Isied, S. S.; Kuo, G.; Raymond, K. N. *J. Am. Chem. Soc.* **1976**, *98*, 1763−1767.
(2) Raymond, K. N.; Isied, S. S.; Brown, L. D.; Fronczek, F. R.; Nibert, J. H. *J. Am. Chem. Soc.* **1976**, *98*, 1767−1774.
(3) Cooper, S. R.; Koh, Y. B.; Raymond, K. N. *J. Am. Chem. Soc.* **1982**, *104*, 5092−5102.
(4) Buglyó, P.; Dessi, A.; Kiss, T.; Micera, G.; Sanna, D. *J. Chem. Soc., Dalton Trans.* **1993**, 2057−2063.
(5) Downs, H. H.; Buchanan, R. M.; Pierpont, C. G. *Inorg. Chem.* **1979**, *18*, 1736−1740.

10.1021/ic000298u CCC: $20.00
Published on Web 12/13/2000

electronic structures of Cr tris(catecholate) complexes has important implications in understanding their reactivities in relation to their possible roles in Cr-induced cancers.[17,18]

Experimental Section

CAUTION: *Cr(VI) is carcinogenic, Cr(V) is mutagenic, and the complexes generated may be capable of cleaving DNA.*[18−20] *Appropriate precautions should be taken to avoid skin contact and dust inhalation while handling these chemicals.*

Synthesis of K[Cr(DTBC)$_3$]. A literature method[6] was used to generate the desired product. Further details are contained in the Supporting Information.

Physical Measurements. Measurements were performed both under Ar (Schlenk line) and following exposure to air. UV/visible spectra were acquired in a stoppered quartz cell on a Hewlett-Packard 8452A diode-array spectrophotometer (λ = 300−800 nm; resolution, 2 nm; integration time, 0.2 s). X-band EPR spectra were recorded as reported previously[17] and analyzed using WinEPR.[21] Electrospray mass spectra were obtained from acetonitrile solutions on a Finnigan LSQ mass spectrometer, and the resulting ESMS spectra were simulated using IsoPro 3.0 software.[22] AAS using a Varian SpectrAA 800 flame spectrometer was used to quantify Cr in the sample. Further details are contained in the Supporting Information.

X-ray Absorption Spectroscopy and Data Processing. Cr K-edge spectra were recorded at 9 K on the Australian National Beamline Facility (ANBF, Beamline 20B) at the Photon Factory, Tsukuba, Japan, using conditions reported previously.[23] The data were recorded as fluorescence spectra because noisy XAFS transmission data were obtained due to absorption by the cryostat and the mass of the ligand, which diluted the Cr concentration. Powdered samples were diluted with BN to ~3.5% w/w Cr (AAS) (to reduce self-absorption) in a N_2 drybox and were subsequently pressed into a 1 × 1 cm^2 hole in a 0.5-mm thick Al spacer between two 63.5-μm Kapton tape windows in air, before rapid cooling to liquid N_2 temperature to minimize oxidation. Spectra were the average of five scans taken at different positions on the sample (edge energies differed by <0.1 eV between the scans). The energy was calibrated using a Cr foil standard, with the first inflection point assigned to an energy of 5989 eV.[16] The XFIT software package,[24,25] incorporating the FEFF 4.06[26] and FEFF 6.01[27] algorithms, was used for data analysis, as described previously.[28] Initial coordinates for modeling the XAFS spectra were obtained from XRD data of related compounds.[2,6,8] Further details of the experimental procedures, restraints, and constraints used in the model (Table S1), the final positional parameters (Table S2), and the main pathways contributing to the XAFS (Table S3) are contained in the Supporting Information.

Results

Characterization of K[Cr(DTBC)$_3$]. The peaks at 458, 536, 620, and 804 nm in the UV/visible spectrum (Figure S1) of K[Cr(DTBC)$_3$] in deaerated acetonitrile are consistent with literature data.[6] Such solutions showed an EPR signal at g_{iso} = 1.9725 (LW = 4.1 × 10^{-4} cm^{-1}, Figure S2a, Supporting Information) with ^{53}Cr satellites ($A_{iso}(^{53}Cr)$ = 22.6 × 10^{-4} cm^{-1}). The weak signal at g_{iso} = 2.0045 (doublet, a_{iso} = 2.63 × 10^{-4} cm^{-1}) results from a small amount of free semiquinone.[29] On exposure to air for ~30 min, two Cr EPR signals were detected (Figure S2b) at g_{iso} = 1.9727 (LW ~ 6.5 × 10^{-4} cm^{-1}, $A_{iso}(^{53}Cr)$ = 22.2 × 10^{-4} cm^{-1}) and g_{iso} = 1.9775 (LW = 1.1 × 10^{-4} cm^{-1}), but the signal at g_{iso} = 2.0045 disappeared. Solid K[Cr(DTBC)$_3$] under Ar contained an EPR signal at g = 1.9718 (weak anisotropy, LW ~ 9.2 × 10^{-4} cm^{-1}; Figure S2c) and a weak signal at g = 2.0043 due to free semiquinone.[29] After 24 h of exposure to air, the signal shifted to g = 1.9726 and a new weak signal appeared at g ~ 1.995 (Figure S2d). There was no evidence of $CrCl_3$ contamination (broad signal, LW > 10^{-2} cm^{-1}; g ~ 1.98) in the solid or solution samples.[12,13] Importantly, EPR spectroscopy showed that the solid could be handled in air for short periods without compromising the integrity of the XAS data.

The negative-ion electrospray mass spectrum in degassed acetonitrile (Figure S3a, Supporting Information) contains a major peak at m/z = 712.7 due to [Cr(DTBC)$_3$]$^-$ (confirmed by the isotope pattern, Figure S4, Supporting Information). The tandem mass spectrum of the m/z = 712.7 peak produces a peak for [Cr(DTBC)$_2$]$^-$ at m/z = 492.4 due to the loss of a neutral ligand.

X-ray Absorption Spectroscopy. The XANES spectrum (Figure 1) of K[Cr(DTBC)$_3$] shows the Cr K-edge at 6003.3 eV and the symmetry-forbidden preedge 1s → 3d peak[15,30] at 5992.9 eV with a peak height of ~8% of that of the edge. The edge energy is intermediate between those for the Cr(V) and Cr(III) complexes of ehba[31] (ehbaH$_2$ = 2-ethyl-2-hydroxybutanoic acid). The normalized preedge peak heights increase as

(6) Sofen, S. R.; Ware, D. C.; Cooper, S. R.; Raymond, K. N. *Inorg. Chem.* **1979**, *18*, 234−239. Upon exposure to air, the solution darkened from mauve to a deeper purple, before becoming pale green after 20 min. The UV/visible spectrum of the green solution exhibited peaks similar to those in the initial spectrum, but a further peak appeared at ~400 nm (Figure S1, Supporting Information). The spectrum of the oxidized species was not consistent with that reported previously for the neutral species, [Cr(DTBC)$_3$].

(7) Gordon, D. J.; Fenske, R. F. *Inorg. Chem.* **1982**, *21*, 2907−2915.

(8) Chang, H.-C.; Ishii, T.; Kondo, M.; Kitagawa, S. *J. Chem. Soc., Dalton Trans.* **1999**, 2467−2476.

(9) Pierpont, C. G.; Downs, H. H. *J. Am. Chem. Soc.* **1976**, *98*, 4834−4838.

(10) Farrell, R. P.; Lay, P. A. *Comments Inorg. Chem.* **1992**, *13*, 133−175.

(11) Barr-David, G.; Charara, M.; Codd, R.; Farrell, R. P.; Irwin, J. A.; Lay, P. A.; Bramley, R.; Brumby, S.; Ji, J. Y.; Hanson, G. R. *J. Chem. Soc., Faraday Trans.* **1995**, *91*, 1207−1216.

(12) Cotton, F. A.; Wilkinson, G. *Advanced Inorganic Chemistry*; 5th ed.; John Wiley & Sons: New York, 1988.

(13) Larkworthy, L. F.; Nolan, K. B.; O'Brien, P. In *Comprehensive Coordination Chemistry*; Wilkinson, G., Gillard, R. D., McCleverty, J. A., Eds.; Pergamon Press: Oxford, U.K., 1987; Vol. 3, pp 699−969.

(14) Solodovnikov, S. P.; Sarbasov, K.; Tumanskii, B. L.; Prokof'ev, A. I.; Vol'eva, V. B.; Bubnov, N. N.; Kabachnik, M. I. *Izv. Akad. Nauk SSSR, Ser. Khim.* **1984**, *8*, 1789−1794.

(15) Ellis, P. J.; Joyner, R. W.; Maschmeyer, T.; Masters, A. F.; Niles, D. A.; Smith, A. K. *J. Mol. Catal. A: Chem.* **1996**, *111*, 297−305.

(16) Arčon, I.; Mitrič, B.; Kodre, A. *J. Am. Ceram. Soc.* **1998**, *81*, 222−224.

(17) Pattison, D. I.; Lay, P. A.; Davies, M. J. *Inorg. Chem.* **2000**, *39*, 2729−2739.

(18) Pattison, D. I.; Lay, P. A.; Davies, M. J. *Redox Rep.* **2000**, *5*, 130−132; Pattison, D. I.; Davies, M. J.; Levina, A.; Dixon, N. E.; Lay, P. A. *Chem. Res. Toxicol.*, submitted.

(19) Farrell, R. P.; Judd, R. J.; Lay, P. A.; Dixon, N. E.; Baker, R. S. U.; Bonin, A. M. *Chem. Res. Toxicol.* **1989**, *2*, 227−229.

(20) *IARC. Monographs on the Evaluation of the Carcinogenic Risk of Chemicals to Humans. Chromium, Nickel and Welding*; IARC: Lyon, France, 1990; Vol. 49.

(21) *WINEPR*, version 960801; Bruker-Franzen Analytic GmbH: Bremen, 1996.

(22) Senko, M. *IsoPro 3.0*; Sunnyvale, CA, 1998.

(23) Codd, R.; Levina, A.; Zhang, L.; Hambley, T. W.; Lay, P. A. *Inorg. Chem.* **2000**, *39*, 990−997.

(24) Ellis, P. J.; Freeman, H. C. *J. Synchrotron Radiat.* **1995**, *2*, 190−195.

(25) *XFIT for Windows'95*; Australian Synchrotron Research Program: Sydney, Australia, 1996.

(26) Mustre de Leon, J.; Rehr, J. J.; Zabinsky, S. I.; Albers, R. C. *Phys. Rev. B* **1991**, *44*, 4146−4156.

(27) Rehr, J. J.; Albers, R. C.; Zabinsky, S. I. *Phys. Rev. Lett.* **1992**, *69*, 3397−3400.

(28) Rich, A. M.; Armstrong, R. S.; Ellis, P. J.; Feeman, H. C.; Lay, P. A. *Inorg. Chem.* **1998**, *37*, 5743−5753.

(29) Sealy, R. C.; Puzyna, W.; Kalyanaraman, B.; Felix, C. C. *Biochim. Biophys. Acta* **1984**, *800*, 269−276.

(30) Bajt, S.; Clark, S. B.; Sutton, S. R.; Rivers, M. L.; Smith, J. V. *Anal. Chem.* **1993**, *65*, 1800−1804.

(31) Levina, A.; Foran, G. J.; Lay, P. A. *J. Chem. Soc., Chem. Commun.* **1999**, *23*, 2339−2340.

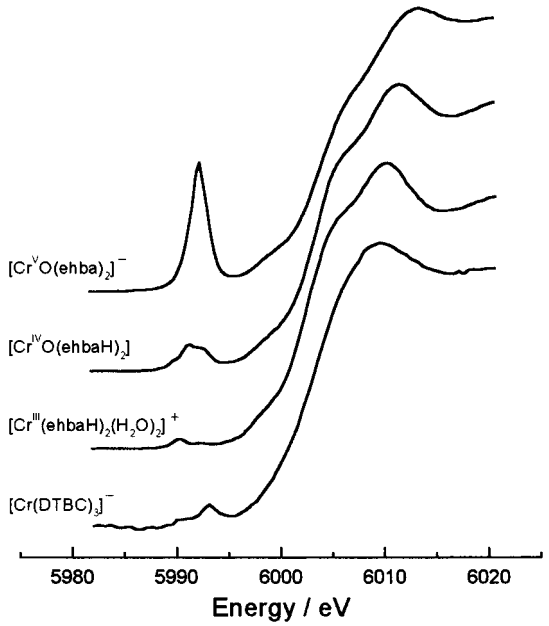

Figure 1. The XANES spectrum for K[Cr(DTBC)$_3$] and comparison with those of Cr−ehba complexes in various oxidation states.

Table 1. Summary of the K-Edge and Preedge Energies and Relative Intensities for [Cr(DTBC)$_3$]$^-$ and the Series of Cr−ehba Complexes with Cr(III/IV/V)

	energy/eV		intensity (% of main edge)[a]
	main edge	preedge peak	
$[Cr(DTBC)_3]^-$	6003.3	5992.9	8.5
$[Cr^{III}(ehbaH)_2(H_2O)_2]^+$ [b]	6002.7	5990.4	4
$[Cr^{IV}O(ehbaH)_2]$[b]	6003.9	5992.2	8.5
$[Cr^{V}O(ehba)_2]^-$ [b]	6004.4	5992.4	46

[a] Intensity measured by height relative to the highest absorption peak. [b] From ref 31.

the oxidation state increases, because of the decrease in symmetry of the complexes and/or an increase in π bonding compared to Cr(III).[30] The normalized preedge peak intensity for K[Cr(DTBC)$_3$] is also intermediate between those expected for Cr(V) and Cr(III) complexes (Figure 1, Table 1).

Single-scattering analyses of the XAFS gave Cr−O bond lengths that were consistent with X-ray structural data (see Supporting Information), but a multiple-scattering (MS) model (Figure 2 and Supporting Information) was used to obtain a better fit to the data, and to confirm the identity of K[Cr(DTBC)$_3$]. Several important MS paths, involving the catechol ring carbons, and even the *tert*-butyl carbons (Table S3) were apparent, but the major scattering pathways were 2-leg paths to the coordinated oxygen atoms (0 → 2 → 0 was the most important path). The 2-leg paths to C13 and C7 were also important (21.2% contribution relative to the most important path). More distant catechol carbons were important in the 3- and 4-leg paths (e.g., 0 → 21 → 20 → 0, 20.3% and 0 → 14 → 15 → 4 → 0, 15.9%). The *tert*-butyl carbons also contributed to some of the more important 4-leg paths (e.g., 0 → 29 → 4 → 0, 8.2%). The best fit to the data (Figure 3; R = 19.8%; good fits typically have R < 20%;[32] Table S2) gave bond lengths and angles within experimental error of the crystallographic data for the same oxidation state for $[Cr(X_4C_6O_2)_3]^-$ (X = Cl or Br),[8] and differ from that for other oxidation states, $[Cr(C_6H_4O_2)_3]^{3-}$,[2] [Cr(DTBC)$_3$],[6] and $[Cr(Cl_4C_6O_2)_3]$[9] (Table 2).

(32) Binsted, N.; Strange, R. W.; Hasnain, S. S. *Biochemistry* **1992**, *31*, 12117−12123. The overdeterminancy (N_i/p) for the model was calculated as 1.19, which shows that the number of independent data points (N_i) is greater than the number of independent parameters (p), allowing a meaningful solution to be obtained.

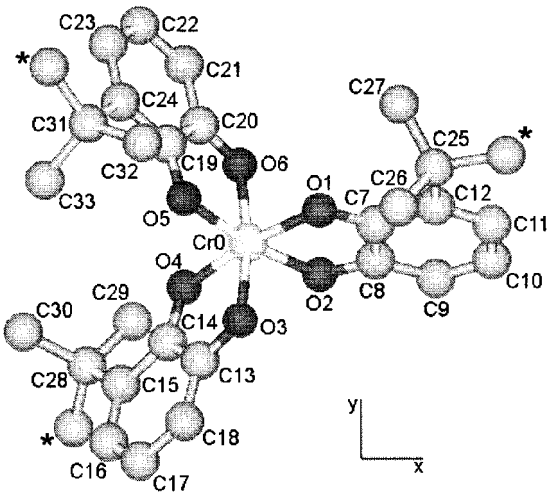

Figure 2. The model of K[Cr(DTBC)$_3$] used to fit the observed XAFS spectra. The axes are shown, with the view looking directly down the z-axis (three-fold axis). The *tert*-butyl groups in the 5-positions (not shown) and the carbons marked with asterisks are not included in the model, as they are farther than 5.2 Å from the metal center and would not contribute significantly to the refinement.

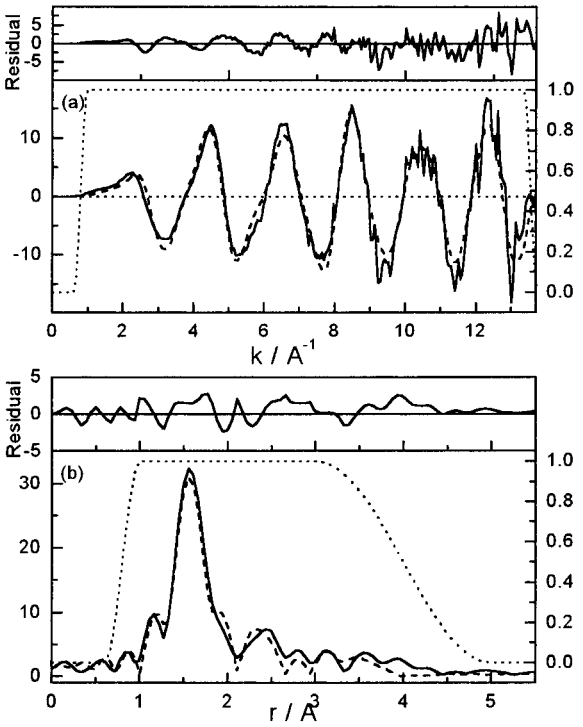

Figure 3. The results of MS fitting, using the model shown in Figure 2, to simulate (a) the XAFS spectrum of solid K[Cr(DTBC)$_3$] and (b) its Fourier transform. Solid lines are the windowed observed spectra; dashed lines represent the windowed calculated spectra; and the dotted lines show the windows for the calculations. The residues from the fit to the data are shown above the spectra with solid lines.

Discussion

The anisotropy observed in the EPR spectra of the solid sample is consistent with the lowest-field peak reported for ^{53}Cr-enriched (98%) [Cr(3,5-DTBC)$_3$]$^-$ in frozen methanol solution,[33] and that of [Cr(3,6-DTBC)$_3$]$^-$ in THF solution (273−293 K).[14]

Table 2. Summary of the Bond Lengths and Angles Determined for K[Cr(DTBC)$_3$] by XAFS and Comparison with X-ray Crystallographic Data for Similar Complexes

parameter[a]	optimized[b] [Cr(DTBC)$_3$]$^-$	[Cr(Cl$_4$C$_6$O$_2$)$_3$]$^-$ [c] Co^{III}Cp$_2^+$	[Cr(Br$_4$C$_6$O$_2$)$_3$]$^-$ [c] TMT-TTF$^{+\bullet}$	[Cr(Br$_4$C$_6$O$_2$)$_3$]$^-$ [c] TMTSF$^{+\bullet}$	[Cr(DTBC)$_3$][d]	[Cr(Cl$_4$C$_6$O$_2$)$_3$][e]	[Cr(O$_2$C$_6$H$_4$)$_3$]$^{3-}$ [f]
Cr−O1	1.96(2)	1.94(1)	1.95(2)	1.94(2)	1.933(8)	1.949(7)	1.986(9)
O1−C7	1.28(2)	1.301(8)	1.29(3)	1.30(2)	1.29(1)	1.280(9)	1.349(5)
C7−C8	1.46(2)	1.423(6)	1.43(3)	1.43(3)	1.433(9)	1.44(1)	1.411(6)
C7−C12	1.42(2)	1.403(8)	1.42(3)	1.40(3)	1.41(1)	1.41(1)	1.388(6)
C9−C10	1.36(2)	1.373(7)	1.38(3)	1.39(3)	1.37(1)	1.36(2)	1.391(7)
C10−C11	1.42(2)	1.403(7)	1.40(3)	1.41(4)	1.41(1)	1.43(1)	1.371(7)
O1−Cr−O2	82(2)	82.6(6)	83(1)	83(1)	81.4(2)	81.8(4)	83.6(2)
Cr−O1−C7	113(2)	112.3(4)	112(1)	113(1)	114.3(6)	113.3(7)	110.7(4)
O1−C7−C8	116(2)				115(1)	115.8(8)	117.2(5)

[a] The values given are weighted averages of all equivalent bond lengths (Å) or angles (deg). [b] The errors given are the systematic errors associated with the XAS technique. Errors due to noise were less significant (see Table S2). [c] From ref 8; TMT-TTF = tetrakis(methylsulfanyl)tetramethylfulvalene; TMTSF = tetramethyltetraselenafulvalene. [d] From ref 6. [e] From ref 9. [f] From ref 2.

This anisotropy is rationalized from the distortions from an octahedral geometry in the XRD structures of [Cr(X$_4$C$_6$O$_2$)$_3$]$^-$ (X = Cl or Br),[8] which have O−Cr−O angles ∼80° due to the constraint of the ligands and ∼50° trigonal twist angles for [Cr(DTBC)$_3$][6] and [Cr(O$_2$C$_6$H$_4$)$_3$]$^{3-}$.[2]

The correspondence of the structure obtained from the best fit of the XAFS data with the XRD structures published for [Cr(X$_4$C$_6$O$_2$)$_3$]$^-$ (X = Cl or Br, Table 2),[8] together with the spectroscopic data, confirms that the features observed in the XANES spectrum are due to [Cr(DTBC)$_3$]$^-$. These features are not consistent with either a pure Cr(III) or Cr(V) complex, with the edge position and the preedge peak intensity being more consistent with a Cr(IV) species. However, known Cr(IV) complexes are unstable in the presence of water at pH > 4[34] and the EPR spectrum is characteristic of a Cr(V) species.[10,11] Thus the complex is best described as a Cr(V) center with a degree of electron delocalization onto the metal center from the ligands. This is consistent with previous proposals[6] that the unpaired electron resides in a molecular orbital that is delocalized over the metal center and the ligands.

The pattern of bond lengths within the ligand and the Cr−O bond lengths are also consistent with a Cr(V) complex in which there is considerable Cr−O π bonding. In particular, if the previous description of a Cr(III) complex with two semiquinone ligands was correct, the Cr−O bond lengths (Table 2) would be expected to be longer in the monoanionic complexes[8] than in [Cr^{III}(O$_2$C$_6$H$_4$)$_3$]$^{3-}$,[2] since catecholato ligands are stronger donors than semiquinones. Clearly, the opposite is the case and is consistent with a higher Cr oxidation state for the 1− complexes[8] compared to the 3− complex.[2] The pattern of bond lengths within the ligand can also be rationalized assuming π donation from the catecholate ligand to Cr(V), since this removes electron density from the HOMO to the metal center. Thus the EPR, XANES, and structural data are most consistent with a model in which there is considerable π donation within a [Cr^{V}(catecholato)$_3$]$^-$, rather than a [Cr^{III}(catecholato)(semiquinone)$_2$]$^-$, structure. This interpretation corroborates the 3.7+ charge calculated for Cr in [Cr^{V}(3,6-DTBC)$_3$]$^-$,[14] which would be less than 3+ for the alternative Cr(III) model. For the latter model, the intensity and energy of the preedge would be expected to be similar to those for octahedral complexes such as [Cr^{III}(ehbaH)$_2$(H$_2$O)$_2$]$^+$, which is clearly not the case. The intensity of the preedge of [Cr^{V}(3,5-DTBC)$_3$]$^-$ is accounted for by a combination of the distortion from an octahedron and the delocalization of the M−L orbitals, which both mix the p and d orbitals and relax the symmetry-forbidden selection rule for the 1s → 3d transitions.

The EPR signals previously assigned to [Cr^{III}(semiquinonato)$_2$(catecholato)]$^+$ [5,33] at g_{iso} = 1.972 decay fairly rapidly in Cr(VI)/catechol(amine) reactions concomitant with the growth of [Cr^{V}O(catecholato)$_2$]$^-$ signals.[17] Together with the EPR and XRD structures of the 1+ species, such results are also indicative of Cr(V) complexes, since inert Cr(III)[12] is not likely to convert to a Cr(V) species. This is important since both the [Cr(catecholato)$_3$]^n (n = 1+, 0) complexes are intermediates in the redox reactions of catechol(amine)s with carcinogenic Cr(VI) complexes[17] and, therefore, an understanding of their chemical and physical properties in relation to their potential genotoxic effects is required.

In conclusion, XRD and XAS and EPR spectroscopic data are most consistent with [Cr(cat)$_3$]^n (n = 1+, 0, 1−) species being Cr(V) complexes with some ligand−metal electron delocalization, rather than Cr(III) complexes.

Acknowledgment. We thank the University of Sydney Cancer Research Fund and the Australian Research Council (QEII fellowship, M.J.D.; large grant, P.A.L.; and RIEFP grants for the EPR spectrometers, ESMS equipment, and 10-element Ge detector) for support. X-ray absorption spectroscopy was performed at the Australian National Beamline Facility (ANBF) with support from the Australian Synchrotron Research Program, which is funded by the Commonwealth of Australia under the Major National Research Facilities program. We thank Mr. Colin Weeks (University of Sydney), Dr. Gary Foran and Dr. James Hester (ANBF) for assistance with acquisition of the XAS data and helpful discussions, and Dr. Xiaomin Song (University of Sydney) for assistance with the ESMS measurements.

Supporting Information Available: Text giving further experimental detail, analysis of the ESMS, and SS and MS analyses of the XAFS. Table S1, summary of the restraints and constraints used in the XAFS model. Table S2, final positional parameters for the XAFS model. Table S3, main MS pathways observed in the XAFS model. Figure S1, UV/visible absorption spectra of K[Cr(DTBC)$_3$]. Figure S2, solid and solution EPR spectra of K[Cr(DTBC)$_3$]. Figure S3, negative-ion electrospray mass spectra of K[Cr(DTBC)$_3$]. Figure S4, observed and simulated ESMS isotope patterns for [Cr(DTBC)$_3$]$^-$. Figure S5, observed and simulated ESMS isotope patterns for some of the dimeric and aggregated species. This material is available free of charge via the Internet at http://pubs.acs.org.

IC000298U

(33) Branca, M.; Fruianu, M.; Sau, S.; Zoroddu, M. A. *J. Inorg. Biochem.* **1996**, *62*, 223−230.
(34) Codd, R.; Lay, P. A.; Levina, A. *Inorg. Chem.* **1997**, *36*, 5440−5448.